Emergence of Unitarity and Locality from Hidden Zeros at One-Loop Order

Jeffrey V. Backus[1,*] and Laurentiu Rodina[2,†]

[1]*Joseph Henry Laboratories, Princeton University, Princeton, New Jersey 08544, USA*

[2]*Beijing Institute of Mathematical Sciences and Applications (BIMSA), Beijing 101408, China*

(Received 8 May 2025; revised 28 August 2025; accepted 3 September 2025; published 22 September 2025)

Recent investigations into the geometric structure of scattering amplitudes have revealed the surprising existence of "hidden zeros": secret kinematic loci where tree-level amplitudes in $\mathrm{Tr}(\phi^3)$ theory, the nonlinear sigma model (NLSM), and Yang-Mills theory vanish. In this Letter, we propose the extension of hidden zeros to one-loop order in $\mathrm{Tr}(\phi^3)$ theory and the NLSM using the "surface integrand" technology introduced by Arkani-Hamed *et al.* We demonstrate that, under the assumption of locality, one-loop integrands in $\mathrm{Tr}(\phi^3)$ are unitary if and only if they satisfy these loop hidden zeros. We also present strong evidence that the hidden zeros themselves contain the constraints from locality, leading us to conjecture that the one-loop $\mathrm{Tr}(\phi^3)$ integrand can be fixed by hidden zeros from a generically nonlocal, nonunitary *Ansatz*. Near the one-loop zeros, we uncover a simple factorization behavior and conjecture that NLSM integrands are fixed by this property, also assuming neither locality nor unitarity. This Letter represents the first extension of such uniqueness results to loop integrands, demonstrating that locality and unitarity emerge from other principles even beyond leading order in perturbation theory.

DOI: 10.1103/7lwk-m5yb

Introduction—Scattering amplitudes provide fascinating insights into the structure of quantum field theory (QFT). The bootstrap approach, which seeks to bypass traditional off-shell methods by determining amplitudes directly from imposing a set of basic physical principles, has emerged as a powerful framework in their study—uncovering unexpected simplicity, efficient computational techniques, and novel mathematical structures. Such remarkable findings are persistent across a broad range of theories, from scalar theories like $\mathrm{Tr}(\phi^3)$ and the nonlinear sigma model (NLSM) to Yang-Mills and gravity. (See Refs. [1,2] for reviews.)

A natural objective within this bootstrap perspective is to identify the minimal set of constraints sufficient to uniquely determine scattering amplitudes. Recently, a series of uniqueness theorems has revealed that the physical principles used to constrain amplitudes often constitute an *overdetermined* system [3–9], implying that naively distinct physical principles are, in fact, *not* independent. Most surprisingly, unitarity (and, in some cases, locality) were shown to emerge for free from other, purely on-shell principles.

The latest addition to this suite of defining principles is the "hidden zeros" [10]—specific kinematic configurations of external particle degrees of freedom where amplitudes vanish [11–16]. This property, totally obscured in the Feynman formulation, is remarkably generic (see, e.g., Refs. [17–22].). In earlier Letter [9], it was proved that tree-level amplitudes in $\mathrm{Tr}(\phi^3)$ theory are uniquely determined by hidden zeros under the assumption of locality, with unitarity an automatic consequence.

One of the greatest challenges in this uniqueness program has been extending these results beyond tree level. If locality and unitarity are indeed to be regarded as emergent properties, it is crucial that we demonstrate this beyond leading order. However, finding such a uniqueness theorem at loop integrand level was previously considered not only difficult but fundamentally ill-defined. The notion of a unique loop integrand is ambiguous for two reasons: (i) internal loop momenta tailored to individual Feynman diagrams can be changed arbitrarily without affecting the physical amplitude, and (ii) in massless theories, one manually tosses out "$1/0$" terms arising from tadpole and external bubble contributions, artificially destroying any single-loop cut structure in the integrand.

It is well known that one can ameliorate the first issue by working in the planar limit. Recently, "surface kinematics" [23–30] has provided a solution to the second issue. With this canonical "surface integrand," there is a natural means of accommodating contributions from tadpoles and external bubbles, in such a way that all single-loop cuts precisely match the expected tree amplitudes with totally generic kinematics.

*Contact author: jvabackus@princeton.edu

†Contact author: laurentiu.rodina@gmail.com

In this Letter, taking as example $\mathrm{Tr}(\phi^3)$ theory and the NLSM, we show that these surface integrands can indeed be uniquely fixed at one-loop order, with both locality and unitarity emerging from purely on-shell constraints. To do this, we first describe the kinematic mesh that neatly organizes kinematic data relevant for one-loop surface integrands [31]. We then propose the one-loop generalization of the hidden zeros discovered at tree level in Ref. [10]. Quite nicely, these zeros are maximal triangles ("big mountains") on the one-loop mesh, in analogy to maximal rectangles on the tree-level mesh. In fact, our approach demonstrates that the various shapes of tree-level zeros have a *unified* origin in different single-loop cuts of surface integrands.

Near these big mountains, we describe a one-loop factorization pattern in both $\mathrm{Tr}(\phi^3)$ and the NLSM, generalizing those found at tree level in Ref. [10]. This discovery adds to an ever-expanding list of factorization behaviors not anticipated from the requirements of unitarity [26,32–35]. With these results in hand, we prove that, under the assumption of locality, the $\mathrm{Tr}(\phi^3)$ integrand is unitary *if and only if* it satisfies the big mountain zeros. We then present strong evidence that big mountain zeros are still sufficient to uniquely determine the $\mathrm{Tr}(\phi^3)$ integrand even without assuming locality.

Finally, we find hidden zeros alone are not sufficient to fully fix the NLSM integrand, a conclusion similar to previous findings involving Adler-like zeros [36,37]. Instead, we conjecture that, assuming neither locality nor unitarity, the stronger requirement of factorization near zeros uniquely fixes the NLSM integrand.

Review: The kinematic mesh and zeros at tree level—In scalar theories, the kinematic data for an n-point scattering amplitude is specified by the momenta of all external particles k_i^μ, satisfying momentum conservation and the on-shell condition. The scattering amplitude is then a rational function of Lorentz-invariant products of these momenta $k_i \cdot k_j$. In theories with *colored* scalars, we can decompose the full amplitude into a sum over color-ordered amplitudes, each of which only receives contributions from planar diagrams. Any of these "partial amplitudes" can then be written solely in terms of the planar variables $X_{i,j} = (k_i + k_{i+1} + \cdots + k_{j-1})^2$. In the present Letter, we treat the X's as a linearly independent set; due to Gram determinant conditions, this implies that we are always working in $d > n-2$ dimensions for an n point.

Nonplanar invariants $c_{i,j} = -2k_i \cdot k_j$ for i, j not adjacent are related to the planar variables by the relation $c_{i,j} = X_{i,j} + X_{i+1,j+1} - X_{i,j+1} - X_{i+1,j}$.

The kinematic data for an n-point scattering process can be encoded in the tree-level "momentum disk" (left-hand side of Fig. 1). The boundary has n marked points, with segments labeled by null external momenta. Each triangulation corresponds to a $\mathrm{Tr}(\phi^3)$ Feynman diagram, with chords $X_{i,j}$ as inverse propagators, and the amplitude follows by summing over all triangulations. NLSM amplitudes instead arise from even angulations of the disk [25].

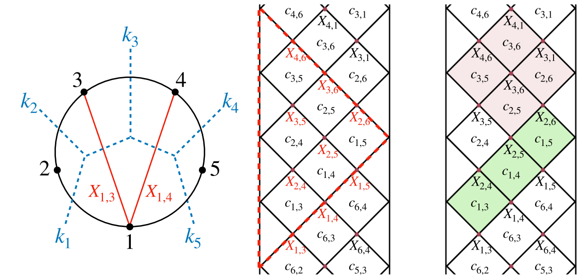

FIG. 1. Left to right: the momentum disk at five points, the six-point kinematic mesh, and examples of zeros on the mesh.

Planar and nonplanar data can also be organized using the tree-level "kinematic mesh" [31] (right-hand side of Fig. 1). Each mesh vertex corresponds to an X, and each diamond is labeled by a $c_{i,j}$ whose indices match the $X_{i,j}$ at its base. The relation for $c_{i,j}$ is obtained by summing the two X's at the top and bottom of the diamond and subtracting the two on the sides.

In Ref. [10], it was shown that color-ordered amplitudes in $\mathrm{Tr}(\phi^3)$ and the NLSM vanish when all c's in any maximal rectangle on the mesh are set to zero (the "hidden zeros"). We can categorize these as (k, m) zeros, each corresponding to the set:

$$\begin{aligned} c_{i,j} = 0, \qquad & i \in \{m, m+1, \ldots, m+k-1\}, \\ & j \in \{k+m+1, k+m+2, \ldots, m-2+n\}. \end{aligned} \tag{1}$$

See Fig. 1 for examples.

Locality requires all singularities to be simple poles in planar invariants $X_{i,j}$, with two X's appearing together only if their chords on the momentum disk do not cross. Unitarity, via the optical theorem, demands that the residue on any pole factorizes into a product of lower-point amplitudes.

Reference [9] proved that imposing $n-3$ $(1, m)$ zeros on a local *Ansatz* restricts us to the $\mathrm{Tr}(\phi^3)$ amplitude, up to an overall normalization. This ensures unitarity on every cut, showing that tree-level unitarity follows *automatically* from hidden zeros and locality.

The kinematic mesh and zeros at one loop—Let us now see how this surface picture extends to loop level. In scalar theories, the loop *integrand* is a rational function of external and loop momenta. In the planar limit, one can construct a canonical one-loop *surface* integrand in $\mathrm{Tr}(\phi^3)$ and the NLSM endowed with both a momentum disk and a kinematic mesh, which we now describe.

At one loop, the analog of the tree-level momentum disk is the *punctured* momentum disk, as shown in Fig. 2. The inclusion of the puncture z introduces some new properties of chords on this surface not present at tree level but critical to describing the surface integrand. For example, using the

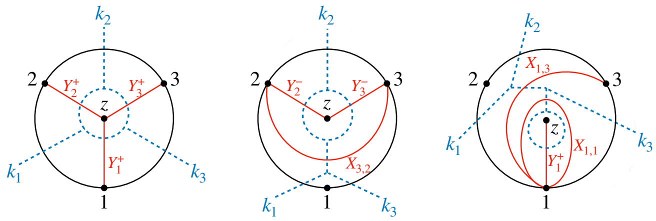

FIG. 2. The one-loop surface picture for kinematic variables and dual Feynman diagrams in $\mathrm{Tr}(\phi^3)$ theory, including vertex corrections (left), external bubbles (middle), tadpoles (right).

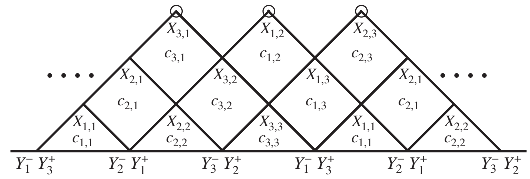

FIG. 3. The Y^-Y^+ mesh at three points.

convention that $X_{i,j}$ denotes a chord that wraps around the puncture in increasing order from i to j (when $i, j \neq z$), it is clear from the surface picture that $X_{i,j} \neq X_{j,i}$, even though naively by "momentum homology" these two should be equal. (We say that two curves are identified via momentum homology when, upon deforming both curves to the boundary of the disk, they are assigned the same momentum dependence. Hence, $X_{i,j}$ and $X_{j,i}$ are momentum homologous, precisely because the puncture does not carry any momentum.) What is more, the surface includes curves that obviously *vanish* by homology, such as the chords $X_{i,i}$ that start on i, wrap around the puncture once, and return to i. (See the right-hand side of Fig. 2 for an example.)

On the other hand, the puncture introduces new variables $X_{i,z} = Y_i$ whose curves start on i and end on the puncture. These are the variables that, when using homology, depend on the internal loop momentum l^μ: fixing, e.g., $Y_1 = l^2$, we have $Y_i = (l + p_1 + \cdots + p_{i-1})^2$ for the rest. For reasons that will become clear in a moment, we will also need to equip the puncture with a parity $Y_i \to Y_i^\pm$, and then take the sum of the integrand with all loop variables positive Y_i^+ and the integrand with all loop variables negative Y_i^- [31].

The surface integrand is defined as a function of this extended kinematic space [27]. This means that we will need to work with variables that vanish in momentum space: each triangulation with a curve $X_{i,i}$ has a tadpole, and those with $X_{i+1,i}$ (and no $X_{i,i}$) have massless external bubbles. To get back to the familiar integrand in momentum space, we can always take away the parity of the puncture, throw out scaleless contributions by hand, set $X_{i,j} = X_{j,i}$, and express the $X_{i,j}$ and Y_i in terms of external momenta k_i^μ and the loop momentum l^μ via homology See the third section of the Supplemental Material [38] for examples of surface integrands.

One can again organize the surface kinematic data using a mesh, an example of which is shown in Fig. 3. Note that the propagator doubling $Y_i \to Y_i^\pm$ is crucial to the construction of the mesh. As at tree level, each (half) diamond in the one-loop mesh corresponds to a nonplanar invariant $c_{i,j}$ whose indices now match those of the planar variable $X_{i,j}$ at the *top* of the diamond. The relationship between the c's and the X's is the same as at tree level, except for $c_{i,i}$ and $c_{i+1,i}$, where we find

$$\begin{aligned} c_{i,i} &= X_{i,i} - Y_i^- - Y_i^+, \\ c_{i+1,i} &= X_{i+1,i} - X_{i,i} - X_{i+1,i+1} + Y_{i+1}^- + Y_i^+. \end{aligned} \quad (2)$$

The zeros on this mesh correspond to setting all c's in a maximal triangle (a "big mountain") to zero. That is, to impose the zero corresponding to the peak labeled by $c_{i-1,i} = 0$, we need to set

$$c_{m,k} = 0, \qquad m \in \{k, k+1, \ldots, i-1\}, \quad (3)$$

for each $k = 1, 2, \ldots, n$. Since these zeros can only be phrased with surface kinematics, their existence is totally inaccessible in a generic integrand written in terms of momenta. In the second section of the Supplemental Material [38], we give the proof that these configurations force integrands in $\mathrm{Tr}(\phi^3)$ and the NLSM to vanish.

Note that we can equally define a mesh with "$-$" and "$+$" switched in Fig. 3, leading to another set of hidden zeros. Hence, the n-point one-loop integrand has $2n$ big mountain zeros. We will denote the zero with peak at $c_{i-1,i} = 0$ and ordering $Y^\pm Y^\mp$ as the $(i, \pm)$ zero of the one-loop mesh. But, there is really a *degeneracy* between the two parities: the integrand satisfies all $(i, +)$ zeros if and only if it satisfies all $(i, -)$ zeros. See the second section of the Supplemental Material [38] for the proof.

As emphasized above, one of the central novelties that surface kinematics buys us is well-defined single-loop cuts. On the punctured disk (as in Fig. 6), a single-loop cut turns chords of an n-point one-loop integrand into chords of an $(n+2)$-point tree amplitude. Complementarily, on the one-loop kinematic mesh, this type of cut isolates a triangular region, corresponding precisely to a ray triangulation of the tree-level $(n+2)$-point mesh (Fig. 8). As we will demonstrate later, the intersection of this triangle with a one-loop mountain zero yields a maximal rectangle, identifying a tree-level zero; see Fig. 7.

Finally, in the surface integrand picture, locality forbids crossing chords on the punctured disk, and unitarity demands consistent factorization on cuts through any set of chords [39].

Factorization near zeros: In Ref. [10], it was shown that, when setting all $c_{i,j}$ to zero in a particular (k, m) zero of the tree-level mesh except one $c_\star \neq 0$, the amplitude in either $\mathrm{Tr}(\phi^3)$ or the NLSM factorizes into two subamplitudes times an overall simple prefactor.

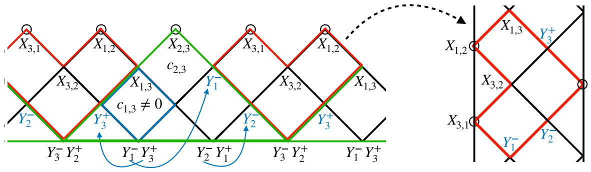

FIG. 4. Factorization of variables near the $(3,-)$ zero at three points. The higher point tree amplitude corresponds to the red-highlighted triangular region. Its kinematic dependence requires replacing some X variables with Y variables, indicated by the blue arrows.

We uncover a similar story at one loop. The mesh itself suggests a natural factorization: deleting any large mountain zero leaves a "ray triangulation" slice of the $(n+2)$-point tree mesh, with the mountain's sides forming its boundaries. Since turning on any $c_\star \neq 0$ inside an $(i,\mp)$ zero enforces $c_\star = -(Y_i^\mp + Y_{i-1}^\pm)$, this points to a factorization of the $\mathrm{Tr}(\phi^3)$ and NLSM integrands as

$$\mathcal{I}_n(c_\star \neq 0) = \left(\frac{1}{Y_i^\mp} + \frac{1}{Y_{i-1}^\pm}\right) \times \mathcal{A}_{n+2}, \tag{4}$$

with tree-level amplitude $\mathcal{A}_{n+2}$ depending on the kinematics in the remaining tree-level mesh with some modifications on its upper and lower boundaries.

For $\mathrm{Tr}(\phi^3)$, this holds exactly. For the NLSM, the picture is subtler. If we treat minus as odd and plus as even in the δ shift (see Ref. [24] for details on the δ shift, and Ref. [40] for a recent extension), the integrand factorizes as in Eq. (4) near $(i,-)$ zeros for even i and near $(i,+)$ zeros for odd i. Factorization at the other zeros requires the opposite-parity prescription (minus even, plus odd). See Fig. 4 for an example and Fig. 5 for the general case. We prove this pattern in Appendix A.

Uniqueness from zeros at one loop in $\mathrm{Tr}(\phi^3)$—

Assuming locality: Let us now prove that the one-loop mesh zeros uniquely fix the color-ordered, *local* (but nonunitary) *Ansatz* for the surface integrand $\mathcal{M}_n$ in $\mathrm{Tr}(\phi^3)$ theory. Below we present only the main steps.

We will start with the same generically nonunitary *Ansatz* as in Ref. [9]: an arbitrary linear combination of all full triangulations of the punctured disk. Taking a single-loop cut of $\mathcal{M}_n$ gives us a nonunitary *Ansatz* for an $(n+2)$-point tree-level amplitude $\mathcal{B}_{n+2}$:

$$\mathrm{Res}_{Y=0}\mathcal{M}_n = \mathcal{B}_{n+2}. \tag{5}$$

In Appendix B, we prove that imposing a big mountain zero on $\mathcal{M}_n$ *secretly* imposes a tree-level zero on $\mathcal{B}_{n+2}$. Concretely, we show that, for the cut on Y_j^+, an $(i,-)$-loop zero acts as an $(i-j-1, j)$-tree zero for any $i = j+2, j+3, \ldots, n+j$. That is, the different zero types at tree level all originate from various combinations of loop zeros and single-loop cuts. Graphically, this can be observed very nicely on the kinematic mesh: the overlap between a mountain zero and the tree mesh induced by the cut is precisely a maximal rectangle, corresponding to a tree-level zero, see Fig. 7.

Then, we find that this set of zeros imposes identical constraints on $\mathcal{B}_{n+2}$ as $(n+2)-3$ distinct $(1,m)$ zeros, which were revealed in Ref. [9] to be sufficient to fix $\mathcal{B}_{n+2}$ to be the *unitary* amplitude $\mathcal{A}_{n+2}$ up to an overall number. See the first section of the Supplemental Material [38] for the proof of the equivalence between the two sets of zeros.

Next, overlap among all cuts with the same parity Y^+ arises from the $1/Y_1^+ \cdots Y_n^+$ term in $\mathcal{M}_n$, forcing all positive-parity terms to carry the same weight a^+. By identical reasoning, negative-parity terms share weight a^-. Since every term in $\mathcal{M}_n$ contains at least one Y, the *Ansatz* reduces to

$$\mathcal{M}_n = a^+\mathcal{I}_n^+ + a^-\mathcal{I}_n^-, \tag{6}$$

where $\mathcal{I}_n^\pm$ denotes the n-point integrand with only $Y^\pm$ poles. In Appendix C, we prove that $a^+ = a^-$ by imposing the $(2,-)$ zero and cutting Y_1^+, a configuration where the tree mesh avoids overlap with the mountain zero.

This proves that n mountain zeros uniquely fix the local *Ansatz* for the one-loop integrand in $\mathrm{Tr}(\phi^3)$ theory; therefore, unitarity follows as an automatic consequence of our assumptions. Since the number of weights in our one-loop *Ansatz* grows exponentially with n, the emergence of unitarity from n hidden zeros and locality is remarkably nontrivial. It turns out that this is really an *equivalence*. See the second section of the Supplemental Material [38], where we prove that unitarity implies the big mountain zeros.

Without assuming locality: Dropping locality, we take an *Ansatz* of all possible n-pole terms built from $X_{i,j}$ or $Y_i^\pm$, no longer corresponding to mesh triangulations, but forbidding factors of both Y^- and Y^+ in the same term. This *Ansatz* grows *factorially* with multiplicity, containing $\sim$6,500 terms at four points. We have verified that big mountain zeros fully fix this one-loop integrand up to four points, allowing us to conjecture that locality and unitarity *both* emerge from hidden zeros at loop level.

Uniqueness from factorization near zeros in the NLSM—We now study uniqueness of the NLSM one-loop integrand. The nonlocal, nonunitary $2n$-point *Ansatz* includes all terms built from any n X or Y variables in numerator and denominator, forbidding opposite-parity Y's in the same term. At four points, the 136 possible XX, XY, and YY factors generate $\sim$25 000 terms.

From four points onward, zeros alone fail to fix the integrand [41]. Instead, we test factorization near zeros. For all $(i,\mp)$ zeros (where plus corresponds to i odd and minus to i even), we require the *Ansatz* satisfies a factorization of the type

$$\mathcal{M}_n(c_* \neq 0) \to \left(\frac{1}{Y_i^{\mp}} + \frac{1}{Y_{i-1}^{\pm}}\right) \times \mathcal{B}_{n+2}^{i,c_\star}(\tilde{X}), \qquad (7)$$

for all $c_* \neq 0$ within those zeros. Here, $B_{n+2}^{i,c_*}(\tilde{X})$ are general *Ansätze* for the $(n+2)$-point tree NLSM amplitude, different for each factorization, and the set $\tilde{X}$ is the X, Y variables consistent with the graphical rule in Fig. 5.

At four points, we have verified that these constraints uniquely reproduce the NLSM integrand, also fixing the left-hand side amplitudes in Eq. (7) in the process. This strongly suggests that factorization near zeros fully determines NLSM integrands at all multiplicities, with both locality and unitarity emerging from this property.

Outlook—In this Letter, we found that one-loop integrands in two scalar theories are uniquely determined by imposing novel constraints: loop hidden zeros and factorization near these zeros. Since our approach assumes neither locality nor unitarity, we have shown that these two seemingly fundamental principles of QFT can be viewed as emergent, even beyond tree level.

Strictly speaking, our proof applies only to a local $\mathrm{Tr}(\phi^3)$ *Ansatz*, where we uncovered the unification of all tree-level zeros in single-loop cuts of the integrand. A natural next step is to prove the same holds even without assuming locality. Another important question is whether any structure of the loop-level zeros survives when returning from surface kinematics to momentum space. Identifying such a feature would likely be nontrivial, but of significant interest.

The surface kinematics framework applies at any loop order [28], and it can also be used to write down a Yang-Mills integrand with well-defined single-loop cuts [27,42]. Thus, a broad range of tests involving uniqueness and emergence from hidden zeros and factorization is now a tangible next step—beyond scalar theories, and at all orders in perturbation theory.

Acknowledgments—It is our pleasure to thank Carolina Figueiredo and Giulio Salvatori for insightful discussions and Nima Arkani-Hamed for helpful comments on the draft. J. V. B. is supported by the NSF Graduate Research Fellowship under Grant No. KB0013612. L. R. is supported by the Beijing Natural Science Foundation International Scientist Project No. IS24014, and the National Natural Science Foundation of China General Program No. 12475070.

Data availability—The data are not publicly available. The data are available from the authors upon reasonable request.

[1] Z. Bern and J. Trnka, arXiv:2210.03146.
[2] G. Travaglini *et al.*, J. Phys. A **55**, 443001 (2022).
[3] N. Arkani-Hamed, L. Rodina, and J. Trnka, Phys. Rev. Lett. **120**, 231602 (2018).
[4] J. J. M. Carrasco and L. Rodina, Phys. Rev. D **100**, 125007 (2019).
[5] L. Rodina, J. High Energy Phys. 09 (2019) 078.
[6] L. Rodina, J. High Energy Phys. 09 (2019) 084.
[7] L. Rodina, Phys. Rev. Lett. **122**, 071601 (2019).
[8] L. Rodina, Phys. Rev. D **102**, 045012 (2020).
[9] L. Rodina, Phys. Rev. Lett. **134**, 031601 (2025).
[10] N. Arkani-Hamed, Q. Cao, J. Dong, C. Figueiredo, and S. He, J. High Energy Phys. 10 (2024) 231.
[11] A. D'Adda, S. Sciuto, R. D'Auria, and F. Gliozzi, Nuovo Cimento Soc. Ital. Fis. **5A**, 421 (1971).
[12] K. Zhou, J. High Energy Phys. 03 (2025) 154.
[13] Y. Li, T. Wang, T. Brauner, and D. Roest, arXiv:2412.14858.
[14] H. Huang, Y. Yang, and K. Zhou, Eur. Phys. J. C **85**, 685 (2025).
[15] Y.-C. Chang, H.-Y. Chen, and Y.-t. Huang, arXiv:2506.15299.
[16] C. R. T. Jones and S. Paranjape, J. High Energy Phys. 07 (2025) 251.
[17] H. Kawai, D. C. Lewellen, and S. H. H. Tye, Nucl. Phys. **B269**, 1 (1986).
[18] Z. Bern, John Joseph M. Carrasco, and H. Johansson, Phys. Rev. D **78**, 085011 (2008).
[19] Z. Bern, John Joseph M. Carrasco, and H. Johansson, Phys. Rev. Lett. **105**, 061602 (2010).
[20] C. Bartsch, T. V. Brown, K. Kampf, U. Oktem, S. Paranjape, and J. Trnka, Phys. Rev. D **111**, 045019 (2025).
[21] Y. Li, D. Roest, and T. ter Veldhuis, J. High Energy Phys. 04 (2025) 121.
[22] S. De, S. Paranjape, A. Pokraka, M. Spradlin, and A. Volovich, J. High Energy Phys. 07 (2025) 174.
[23] N. Arkani-Hamed, H. Frost, G. Salvatori, P.-G. Plamondon, and H. Thomas, J. High Energy Phys. 08 (2025) 194.
[24] N. Arkani-Hamed, Q. Cao, J. Dong, C. Figueiredo, and S. He, Phys. Rev. D **110**, 065018 (2024).
[25] N. Arkani-Hamed and C. Figueiredo, arXiv:2403.04826.
[26] N. Arkani-Hamed and C. Figueiredo, arXiv:2405.09608.
[27] N. Arkani-Hamed, Q. Cao, J. Dong, C. Figueiredo, and S. He, Phys. Rev. Lett. **134**, 171601 (2025).
[28] N. Arkani-Hamed, H. Frost, and G. Salvatori, arXiv:2412.21027.
[29] S. De, A. Pokraka, M. Skowronek, M. Spradlin, and A. Volovich, J. High Energy Phys. 09 (2024) 160.
[30] G. Salvatori, J. High Energy Phys. 12 (2019) 074.
[31] N. Arkani-Hamed, S. He, G. Salvatori, and H. Thomas, J. High Energy Phys. 11 (2022) 049.
[32] F. Cachazo, N. Early, and B. Giménez Umbert, J. High Energy Phys. 08 (2022) 252.
[33] Q. Cao, J. Dong, S. He, C. Shi, and F. Zhu, J. High Energy Phys. 09 (2024) 049; 01 (2025) 126(E).
[34] Y. Zhang, Phys. Rev. D **111**, 085004 (2025).
[35] Y. Zhang, J. High Energy Phys. 02 (2025) 074.
[36] C. Bartsch, K. Kampf, and J. Trnka, Phys. Rev. D **106**, 076008 (2022).
[37] C. Bartsch, K. Kampf, J. Novotny, and J. Trnka, Phys. Rev. D **110**, 045009 (2024).

[38] See Supplemental Material at http://link.aps.org/supplemental/10.1103/7lwk-m5yb for more proof details, and integrand examples.

[39] While these definitions guarantee that the physical loop-integrated amplitude is consistent with locality and unitarity, they constitute strictly stronger requirements, as they include rules for dealing with tadpoles and external bubbles that do not appear post-loop-integration.

[40] S. Paranjape, M. Skowronek, M. Spradlin, and A. Volovich, arXiv:2504.11253.

[41] For the purposes of constructing amplitudes, one practical solution to obtain a unique result is to allow only same-parity terms in the numerator, i.e., only $X_{e,e}$, $X_{o,o}$, and Y_e^+ and Y_o^- (when, for example, assigning $Y^{+/-}$ to be even or odd parity). This eliminates the trivial solutions and gives an efficient bootstrap procedure.

[42] J. V. Backus and C. Figueiredo, J. High Energy Phys. 09 (2025) 069.

End Matter

Appendix A: Factorization proof—Here, we prove the factorization formula (4). To do this, let us fix a particular $(i,-)$ zero and $c_{a,b} \neq 0$ (the "loop near-zero" condition) and impose them on the $\mathrm{Tr}(\phi^3)$ integrand $\mathcal{I}_n$. We can then cut on *any*$Y_j^\pm$, which will produce a particular tree amplitude $\mathcal{A}'_{n+2}$ with generic kinematics on the support of the loop near zero. For the moment, let us restrict our discussion so that we cut on neither Y_i^- nor Y_{i-1}^+. In this case, after imposing the loop near-zero condition, there are two options for $\mathcal{A}'_{n+2}$. If the overlap between the loop and tree meshes (as shown in Fig. 7) contains only c variables that vanish, then $\mathcal{A}'_{n+2} = 0$.

If, alternatively, the overlap contains $c_{a,b} \neq 0$, the tree amplitude will factorize as

$$\mathcal{A}'_{n+2} = \left(\frac{c_{a,b}}{X_\mathrm{B} X_\mathrm{T}}\right) \times \mathcal{A}_\mathrm{down} \times \mathcal{A}_\mathrm{up}, \tag{A1}$$

with right-hand side kinematics given by the rules in Ref. [10]. Looking at Fig. 7, we can easily pick out the universal prefactor for the factorization of $\mathcal{A}'_{n+2}$ in this loop near-zero configuration: it is the four-point tree amplitude with kinematics given by the left-most and right-most corners of the overlap region. When cutting on a Y_j^+, the right-most planar variable is always Y_{i-1}^+. The left-most is $X_{j,i} = Y_i^- + Y_j^+ = Y_i^-$ on the cut. (The same story, with sides reversed, holds for cuts on Y_j^-.) So, we have

$$\mathcal{A}'_{n+2} \to \left(\frac{1}{Y_i^-} + \frac{1}{Y_{i-1}^+}\right) \times \mathcal{R}, \tag{A2}$$

where $\mathcal{R}$ is the product of unimportant lower-point amplitudes. This implies that all terms in $\mathcal{I}_n$ with at least one Y that is neither Y_i^- nor Y_{i-1}^+ is proportional to the prefactor shown in Eq. (4).

When we now cut on Y_i^-, we are left with a tree amplitude $\mathcal{A}_{n+2}^{(1)}$ whose mesh has no overlap with the zero. As such, it will neither vanish nor factorize. As we discuss in Appendix B, the kinematics of $\mathcal{A}_{n+2}^{(1)}$ are precisely those in the tree mesh formed as in Fig. 8 but instead with a shift on its left edge $X_{i-1,m} \to Y_m^-$ for all m. However, on the loop near zero and cut, we also have $X_{m,i} = Y_m^+$ for all $m \leq a-1$ and $Y_m^- = X_{i-1,m}$ when $m < b+1$. Note that this derives, respectively, the rules in the blue and red triangles in Fig. 5. We can proceed with the same arguments for the cut on Y_{i-1}^+, obtaining $\mathcal{A}_{n+2}^{(2)}$ whose tree mesh has the same interior as that of $\mathcal{A}_{n+2}^{(1)}$ and also undergoes the shifts drawn in Fig. 5 on the edges. So, $\mathcal{A}_{n+2} = \mathcal{A}_{n+2}^{(1)} = \mathcal{A}_{n+2}^{(2)}$ on this kinematic configuration.

Thus, we have shown that, on a loop near zero, the integrand is proportional to the prefactor given in Eq. (4), and that this prefactor multiples the tree amplitude $\mathcal{A}_{n+2}$ with kinematics as shown in Fig. 5. So, we have proved Eq. (4) in $\mathrm{Tr}(\phi^3)$ theory. As always, the proof for $(i,+)$ zeros goes through in an identical manner.

In Ref. [10], the analogous tree-level factorization was proved using classic "stringy" integrals that UV-complete $\mathrm{Tr}(\phi^3)$ and NLSM tree-level amplitudes. In this Letter, we instead prove this factorization solely from properties of the "low-energy" field-theory object $\mathcal{I}_n$.

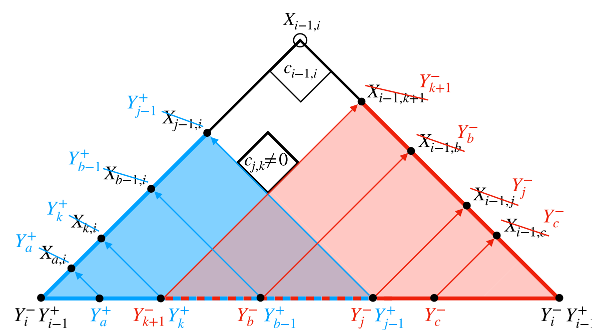

FIG. 5. Factorization of variables near a $(i,-)$ zero with $c_{j,k} \neq 0$. The region below and beside $c_{j,k}$ is divided into blue and red parts. All the X variables on the slope of the mountain in a colored region are replaced with Y variables using the rule shown in the figure.

Appendix B: Loop zeros impose tree zeros on the single-loop cuts—In this appendix, we prove that the loop zeros act as tree zeros on single-loop cuts of the loop-integrand *Ansatz*. We will consider here the $(i,-)$ zeros and the Y^+ cuts. (Different parity choices can be treated identically.) For simplicity, we will focus on cutting Y_1^+. The first thing we must do is prove that the operations of imposing a zero and taking a residue commute, since our assumption is the full integrand vanishes (not individual cuts). As long as $i \neq 2$, we find that

$$\mathrm{Res}_{Y_1^+=0}(\mathcal{M}_n|_{(i,-)}) = \left(\mathrm{Res}_{Y_1^+=0}\mathcal{M}_n\right)_{(i,-),Y_1^+=0}. \qquad \text{(B1)}$$

This is because, for $i \neq 2$, setting $Y_1^+ = 0$ on the support of an $(i,-)$ zero does not force any other kinematic variables to vanish, ensuring the residues on both sides of Eq. (B1) pick up the same terms. To contrast, for $i = 2$ the zero sets $Y_2^- = -Y_1^+$, so the residue on the left-hand side will pick up extra terms as compared to the right-hand side corresponding to the pole in Y_2^-.

Because it is our hypothesis that $\mathcal{M}_n$ satisfies the big mountain zeros, we have the condition

$$\left(\mathrm{Res}_{Y_1^+=0}(\mathcal{M}_n)\right)_{(i,-),Y_1^+=0} = \mathcal{B}_{n+2}(Z_{i,j})|_{(i,-),Y_1^+=0} = 0 \qquad \text{(B2)}$$

for all $i \neq 2$, where $\mathcal{B}_{n+2}$ is our local tree-level *Ansatz* with generic kinematics we denote by $Z_{i,j}$ to distinguish them from the loop $X_{i,j}$. It is simple to work out the mapping between the Z's and the X/Y's: the nontrivial ones are $Y_i^+ \leftrightarrow Z_{i,n+2} = Z_{n+2,i}$, $X_{i,1} \leftrightarrow Z_{i,n+1} = Z_{n+1,i}$, and $X_{1,i} \leftrightarrow Z_{i,1} = Z_{1,i}$ for $i = 2,3,\ldots,n$, and $X_{1,1} \leftrightarrow Z_{1,n+1}$. For the rest, we have $X_{i,j} \leftrightarrow Z_{i,j} = Z_{j,i}$ for $i < j$. (Note that $X_{i,j}$ with $i \geq j$ are always locally inconsistent with the Y_1^+ chord.) We show examples of how this works in Fig. 6.

Now, the local structure of $\mathcal{B}_{n+2}$ in terms of Z variables defines a tree-level mesh which can easily be obtained graphically from the loop mesh, as we show in Fig. 8. Quite beautifully, for any $i \neq 2$, the overlap of an $(i,-)$ zero and the tree mesh of $\mathcal{B}_{n+2}$ is exactly a maximal rectangle—a tree-level hidden zero. (See the blue diamond in Fig. 7.)

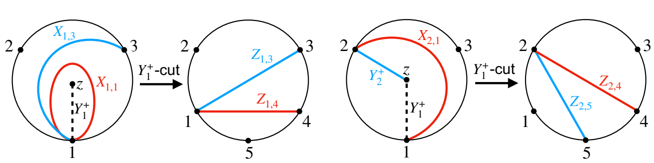

FIG. 6. The Y_1^+ cut of an n-point integrand induces a local triangulation of the $(n+2)$-point tree disk.

For diamonds that do not touch the right edge of the tree mesh, it is clear that the $c_{i,j}(X) = 0$ conditions of the loop zero trivially induce the corresponding $c_{i,j}(Z) = 0$ conditions in the tree mesh. For diamonds that do touch the right edge (but are not the bottom-most diamond), the mountain zero condition $c_{k,1}(X) = 0$ implies that

$$X_{k,1} + X_{k-1,2} = X_{k-1,1} + X_{k,2}. \qquad \text{(B3)}$$

But, we also have $X_{i,2} = Y_i^+ + Y_2^-$ for all $i \leq \max(k)$ on the support of the zero. So, Eq. (B3) is equivalent to $X_{k,1} + Y_{k-1}^+ = X_{k-1,1} + Y_k^+$, which is exactly what appears on the overlap between the tree mesh and loop mesh in Fig. 7. Finally, for the bottom-most diamond, setting $c_{2,1} = 0$ and $Y_1^+ = 0$ tells us

$$X_{2,1} + Y_2^- = X_{1,1} + X_{2,2}. \qquad \text{(B4)}$$

Since we have $X_{2,2} = Y_2^+ + Y_2^-$ on the support of the zero, this condition matches what is shown in Fig. 7.

As a result of these arguments, the fact that $\mathcal{B}_{n+2}$ vanishes on the zero + cut condition shown in Eq. (B2) is *equivalent* to it vanishing on a tree-level hidden zero. In general, for the cut on Y_j^+, an $(i,-)$-loop zero acts as an $(i-j-1, j)$-tree zero for all $i = j+2, j+3, \ldots, n+j$.

Appendix C: Fixing $a^+ = a^-$—Here, we prove that imposing a final zero on

$$\mathcal{M}_n = a^+\mathcal{I}_n^+ + a^-\mathcal{I}_n^- \qquad \text{(C1)}$$

leads to $a^+ = a^-$. To do this, let us impose the $(2,-)$ zero and cut Y_1^+. Note that this is exactly the choice where the tree mesh has no overlap with the mountain zero. On this zero, we have $Y_1^+ = -Y_2^-$, and so we get

$$\left(a^+\mathcal{A}_{n+2}^{(1)} - a^-\mathcal{A}_{n+2}^{(2)}\right)_{(2,-),Y_1^+=0} = 0, \qquad \text{(C2)}$$

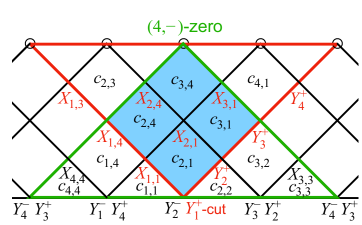

FIG. 7. The mountain zeros (green) intersect the mesh area corresponding to a tree amplitude (red) in maximal rectangular regions, producing the tree-level zeros.

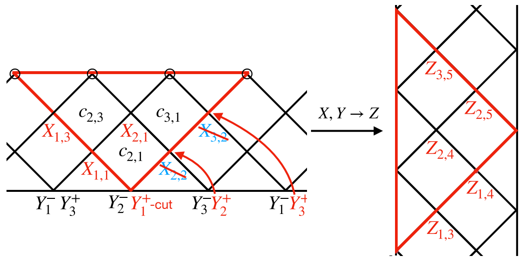

FIG. 8. The Y_1^+ cut defines the ray triangulation of an $(n+2)$-point tree mesh, where the loop-level $X_{i,2}$ on the right edges are replaced with the corresponding Y_i^+.

where $\mathcal{A}_{n+2}^{(1)}$ is the tree amplitude resulting from the cut in Y_1^+ and $\mathcal{A}_{n+2}^{(2)}$ is that for the cut in Y_2^-. Since these Y variables lie at the same point on the loop mesh, the interior of their tree meshes are identical (see Fig. 8); it is only on the edges that they may differ.

However, on the support of the zero + cut conditions, it is straightforward to show that the edges also exhibit identical kinematic dependence. As a result, we find that $\mathcal{A}_{n+2}^{(1)}$ and $\mathcal{A}_{n+2}^{(2)}$ are the *same* amplitude on the support of the zero + cut, and thus $a^+ = a^-$ for Eq. (C2) to hold.